Applied Catalysis B: Environmental 229 (2018) 32–40

Contents lists available at ScienceDirect

Applied Catalysis B: Environmental

journal homepage: www.elsevier.com/locate/apcatb

Enhanced catalytic hydrogenation reduction of bromate on Pd catalyst supported on CeO_2 modified SBA-15 prepared by strong electrostatic adsorption

Jingya Sun[a], Jiarun Zhang[a], Heyun Fu[a], Haiqin Wan[a,*], Yuqiu Wan[a], Xiaolei Qu[a], Zhaoyi Xu[a], Daqiang Yin[b], Shourong Zheng[a,*]

[a] State Key Laboratory of Pollution Control and Resource Reuse, Jiangsu Key Laboratory of Vehicle Emissions Control, School of the Environment, Nanjing University, Nanjing 210093, PR China

[b] Key Laboratory of Yangtze River Water Environment of Ministry of Education, Tongji University, Shanghai 200092, PR China

ARTICLE INFO

Keywords:
CeO2
Modified SBA-15
Supported Pd catalysts
Liquid phase catalytic hydrogenation
Strong electrostatic adsorption
Bromate

ABSTRACT

Supported Pd catalysts on CeO_2 modified SBA-15 (Ce-SBA-15) were prepared using the strong electrostatic adsorption (SEA) method. For comparison, supported Pd catalysts on SBA-15 and Ce-SBA-15 were prepared using the impregnation method. Liquid-phase catalytic hydrogenation of bromate was investigated on those catalysts. The catalysts were characterized by X-ray diffraction, N_2 adsorption-desorption, measurement of the point of zero charge (PZC), transmission electron microscopy, X-ray photoelectron spectroscopy, transmission electron microscopy − energy dispersive spectroscopy, and H_2 chemisorption. Characterization results showed that CeO_2 modification resulted in increased PZC of SBA-15 from 2.7 to 4.8. For Pd/Ce-SBA-15 catalysts prepared using the SEA method, Pd particles were site-specifically deposited on CeO_2 moieties. As a result, much higher Pd dispersion and stronger metal-support interaction were observed as compared with the catalysts prepared using the impregnation method. Furthermore, increasing CeO_2 modification amount and decreasing Pd loading amount effectively enhanced Pd dispersion and metal-support interaction. For the catalytic reduction of bromate, Pd/SBA-15 prepared using the impregnation method exhibited negligible catalytic activity. In contrast, markedly enhanced catalytic activities were observed on Pd catalysts supported on Ce-SBA-15. Additionally, Pd/Ce-SBA-15 prepared using the SEA method displayed much higher activity than that prepared using the impregnation method. For Pd/Ce-SBA-15 prepared using the SEA method, increasing CeO_2 modification amount led to enhanced catalytic activity. The present findings clearly indicate that Pd/Ce-SBA-15 prepared by the SEA method can be used as a promising catalyst in liquid phase catalytic hydrogenation of disinfection byproducts.

1. Introduction

Disinfection byproducts (DBPs), such as bromate, have been proven to be strongly carcinogenic [1]. The United States Environmental Protection Agency (EPA) and World Health Organization (WHO) have issued strict regulations for bromate in drinking water [2,3]. Accordingly, different treatment methods have been developed to eliminate bromate pollution in water, such as biological remediation [4], photocatalysis [5], chemical reduction [6], electrochemical method [7], and so on. As a clean reduction treatment method, liquid phase catalytic hydrogenation has been used for the removal of reducible organic or inorganic pollutants [8–13]. Recent studies showed that bromate-could be removed using liquid phase catalytic hydrogenation [10,13].

Supported noble metal catalysts are commonly used in liquid-phase catalytic hydrogenation [14]. The structural properties and catalytic performances of supported catalysts are strongly dependent on catalyst supports. For example, high Pd dispersion could be obtained on Al_2O_3, ZrO_2 and CeO_2, while large Pd particles (low Pd dispersion) were usually observed on SiO_2 and carbonaceous supports [11,12,15,16]. Furthermore, strong metal-support interactions were usually observed in Pd catalysts supported on ZrO_2 and CeO_2, giving rise to enhanced catalytic activities [11,13,17].

Mesoporous SBA-15 with hexagonally arranged channels and uniform mesopores has been considered as a promising catalyst support due to its high surface area and ordered pore structure [18,19]. For noble metal catalyst supported on mesoporous SiO_2, however, large noble metal particles and low dispersion were normally observed due to very weak metal-support interactions. In liquid phase catalytic

* Corresponding authors.
E-mail addresses: wanhq@nju.edu.cn (H. Wan), srzheng@nju.edu.cn (S. Zheng).

https://doi.org/10.1016/j.apcatb.2018.02.009
Received 31 August 2017; Received in revised form 21 January 2018; Accepted 4 February 2018
Available online 06 February 2018

reactions, catalytic activities are closely related to the adsorption of reactants on the catalysts surface [20]. Because of their very low PZC (*e.g.*, 1.9–4.0) [21,22], mesoporous SiO_2 supported catalysts usually displayed very low catalytic activities for the catalytic conversion of anionic pollutants because the adsorption of anionic reactants was strongly suppressed due to electrostatic repulsive interaction between negatively charged SiO_2 and anionic pollutant. Recent studies showed that the catalytic performances of mesoporous SiO_2 supported catalysts could be improved by modification using metal oxides (*e.g.*, CeO_2, TiO_2 and Fe_2O_3) in some catalytic systems, such as CO oxidation, steam reforming and water-gas shift reaction [23–25]. Among the metal oxides, CeO_2 was the most attractive one, which was capable of invoking very strong interactions with noble metals and resulting in high metal dispersion [13,17]. As a result, enhanced catalytic activity could possibly be achieved. It is noteworthy mentioning that from the viewpoint of sustainable utilization of rare earth source CeO_2 is commonly used as a doping agent in catalyst supports due to its increasing supply risk and poor thermal stability [26–28]. Hence, CeO_2 doped SBA-15 was used as the catalyst support instead of CeO_2 in this study.

Strong electrostatic adsorption (SEA) is a facile and effective method to prepare supported metal catalysts with high dispersions [29–31]. It should be emphasized that in CeO_2 modified mesoporous SiO_2, CeO_2 moieties presented in addition to SiO_2 surface. If the conventional impregnation method is adopted for the preparation of supported noble metal catalysts, noble metal may be located randomly on the surface of both CeO_2 and SiO_2 surface. Notably, CeO_2 had a much higher PZC (*i.e.*, 6.5) than SiO_2. We thus hypothesized that controllable preparation of noble metal catalysts supported on CeO_2 modified mesoporous SiO_2 could be implemented using the SEA method. For example, provided that anionic $[PdCl_4]^{2-}$ was used as the Pd precursor, selective adsorption of $[PdCl_4]^{2-}$ on positively charged CeO_2 moieties instead of negatively charged SiO_2 could be expected in a pH range of 2.0–6.5. Eventually, site-specific deposition of Pd particles on CeO_2 moieties could be obtained upon reduction. Hence, we speculated that Pd catalysts prepared by the SEA method may display excellent catalytic activities in liquid-phase catalytic hydrogenation reduction of anionic bromate, while thus far similar studies have not been reported.

The main objective of the present study is to evaluate the catalytic performance of Pd catalysts supported on CeO_2 modified mesoporous SiO_2 for the liquid phase catalytic hydrogenation of bromate. We prepared a series of supported Pd catalysts on CeO_2 modified SBA-15 using the SEA method. For comparison, Pd catalysts supported on SBA-15 and CeO_2 modified SBA-15 were prepared using the impregnation method. The catalysts were characterized and the liquid phase catalytic hydrogenation of bromate was studied. Characterization results showed that highly dispersed Pd species with strong metal-support interactions were obtained on CeO_2 modified SBA-15 prepared by the SEA method. Accordingly, boosted catalytic activities were observed on supported Pd catalysts prepared by the SEA method as compared with those prepared using the impregnation method.

2. Experimental

2.1. Catalyst preparation

Mesoporous SiO_2 (SBA-15) was prepared according to the method previously reported [18]. CeO_2 modified SBA-15 was prepared by the conventional impregnation method. Briefly, SBA-15 was mixed with a desired amount of $Ce(NO_3)_2$ solution, which was stirred vigorously for 2 h before vapored to dry at 90 °C. The obtained samples were dried at 105 °C for 6 h and then calcined at 400 °C for another 6 h. Pd catalysts supported on CeO_2 modified SBA-15 were prepared using the strong electrostatic adsorption (SEA) method. Briefly, CeO_2 modified SBA-15 was suspended in aqueous solution with a desired amount of H_2PdCl_4, and the pH was adjusted to 3.6. After stirring for 24 h, the sample was collected by filtration and washed with distilled water several times, followed by drying in an oven at 105 °C for 6 h. The resultant catalysts were denoted as *ad*-Pd(x)/Ce(y)-SBA-15, where x and y are the contents of Pd and Ce determined by inductive coupled plasma emission spectrometer. For comparison, Pd catalysts supported on CeO_2 modified SBA-15 and SBA-15 were also prepared using the conventional impregnation method, and the resultant catalysts were denoted as *im*-Pd(x)/Ce(y)-SBA-15 and *im*-Pd(x)/SBA-15, respectively. Before characterization and catalytic activity evaluation, the catalysts were calcined at 300 °C for 5 h and reduced by H_2 at 300 °C for 2 h.

2.2. Catalyst characterization

Powder X-ray powder diffraction (XRD) patterns of the samples were recorded on a Rigaku D/max-RA powder diffraction-meter (Rigaku, Tokyo, Japan) using Cu-Kα radiation (λ = 1.540562 Å). The contents of Pd and Ce in the catalysts were measured by inductively coupled plasma emission spectrometer (ICP-AES) on a PerkinElmer Optima-5300DV spectrometer (Perkin-Elmer, Inc., USA). Transmission electron microscopy (TEM) of the samples was performed on a JEM-200CX electron microscope (JEOL Co., Tokyo, Japan). EDS elemental mapping and high-angle annular dark field (HAADF)-TEM were performed on an ARM-200F transmission electron microscope (JEOL Co., Japan.) with an X-MAX energy dispersive spectrometer (Oxford, UK). Brunauer–Emmett–Teller (BET) surface areas of the catalysts were measured using the nitrogen adsorption method on a Micromeritics ASAP 2020 (Micromeritics Instrument Co., Norcross, GA) at −196 °C (77 K). X-ray photoelectron spectroscopy (XPS) was recorded on an ESCALAB 250 (Thermo Scientific, USA) equipped with a monochromatized Al Kα X-ray source (hν = 1486.6 eV) and a hemispherical electron analyzer. The binding energy values were calibrated using the C 1s peak (284.8 eV).

H_2 chemisorption was carried out using a pulse method on a Micromeritics Autochem II chemisorption analyzer (Micromeritics Instrument Co., Norcross, GA) to determine Pd dispersions in the catalysts. Before H_2 adsorption, 20 mg of the samples was placed in a U-shaped quartz reactor and pre-reduced by a 10 vol% H_2/Ar stream at 300 °C for 2 h, followed by purging the sample at 300 °C for 1 h by an Ar stream. After cooling down to 25 °C, H_2 chemisorption was conducted. The dispersion of Pd was calculated by assuming the chemisorption stoichiometry ratio of H_2/Pd is 0.5 [32].

The points of zero charge (PZCs) of SBA-15, CeO_2 and CeO_2 modified SBA-15 were measured by the potentiometric mass titration method [33]. Briefly, 0.1 g of the sample was suspended in 10 ml of 0.01 M NaCl solution. After addition of 0.2 ml of 1.0 M NaOH and equilibration for 24 h, the suspension was titrated using a 0.5 M HCl solution under continuous N_2 bubbling. The blank solution was also titrated following the above process in the absence of sample. The pH values were continuously recorded during the titration process. The pH curves of the samples as a function of the amount of HCl added are shown in Fig. S1, supporting information (SI).

2.3. Liquid phase catalytic hydrogenation

The liquid phase catalytic hydroreduction of bromate at 25 °C under atmospheric pressure of hydrogen was used to evaluate the catalytic performances of the catalysts. For bromate reduction, 10 mg of catalyst was added in a four necked flask having 360 ml of 0.60 mM bromate solution, and solution pH was pre-adjusted to 5.6 using 0.1 M HCl. Under vigorous stirring (1500 rpm), a N_2 flow (200 ml min^{-1}) was used to purge the suspension for 30 min to remove O_2, and the N_2 flow was then switched to H_2 (200 ml min^{-1}) to start the reaction. Samples were taken at preset intervals and filtrated to remove catalyst particles before determination. The concentrations of bromate and bromide in the filtrates were measured on an ion chromatography (ICS1000, Dionex, USA) using 10 mM KOH solution as the mobile phase.

To evaluate the catalytic activities, the initial activities of the

catalysts were used by calculating the rate constants with the conversion below 25% according to the first-order reaction kinetics. The reproducibility of catalytic activity for bromate reduction was verified by two separate reaction runs and results are presented in Fig. S2, SI. Three catalyst dosages (0.014, 0.028 and 0.042 g l^{-1}) were used in the catalytic reduction of bromate to test the potential mass transfer limitations. As shown in Fig. S3b, SI, nearly constant catalytic activities normalized by the catalyst dosage were observed, suggesting the absence of mass transfer limitation under our reaction conditions.

3. Results and discussion

3.1. Catalyst characterization

N_2 adsorption-desorption isotherms and pore size distributions of the samples are presented in Fig. S4, SI. After CeO_2 modification and Pd loading, all samples retained typical type IV adsorption isotherms with standard H1 hysteresis loops in the relative pressure (p/p_0) range of 0.6–0.8, characteristic of the well-reserved regular hexagonal mesoporous structure similar to that of pristine SBA-15. The structural parameters of the samples are listed in Table S1, SI. In comparison with SBA-15, the BET surface areas and the total pore volumes decreased with CeO_2 modification amount, indicative of CeO_2 incorporation into SBA-15 channels [34]. The pore size distributions of the samples were calculated according to the desorption branch of the isotherms using the BJH method. The pore diameters kept almost constant before and after CeO_2 modification and Pd loading, indicative of the unblocked mesopores.

The small angle XRD patterns of SBA-15 and CeO_2 modified SBA-15 are shown in Fig. 1a. All samples displayed three strong diffraction peaks with 2θ around 0.9°, 1.6 °, and 1.9 °, respectively, corresponding to the diffraction of (100), (110) and (200) planes of SBA-15 [18], confirming a well-retained ordered mesostructure after CeO_2 modification. The characteristic (100) peak at 0.9° slightly shifted to high angle (0.95°) and attenuated in intensity with CeO_2 modification amount. The shift of characteristic peak to large angle suggested a slightly decreased unit cell parameter of SBA-15, reflecting an increased thickness of SBA-15 framework wall, likely due to the incorporation of partial CeO_2 particles in the channel of SBA-15 [35]. The large angle XRD patterns of the samples are compiled in Fig. 1. The diffraction peaks observed at 22° in all the samples were characteristic of amorphous silica [36]. Increasing CeO_2 amount led to gradual development of diffraction peaks at 28.5 °, 33.0 °, 47.5 ° and 56.3°, assigned to CeO_2 phase with a fluorite structure [37]. After Pd loading, additional diffraction peak was clearly observed at 40.1o on *im*-Pd(0.94)/SBA-15, corresponding to metallic Pd with a face centered cubic (fcc) structure [37]. In contrast, a weak one at 40.1° was identified on *im*-Pd(0.92)/Ce(4.69)-SBA-15, while similar diffraction peak was not observed on *ad*-Pd(0.91)/Ce(4.69)-SBA-15 (see Fig. 1c). Given similar Pd loading amounts in the catalysts, the results suggested that larger Pd particles presented on SBA-15 and a higher metal dispersion was observed on *ad*-Pd(0.91)/Ce(4.69)-SBA-15. For *ad*-Pd/Ce-SBA-15 catalysts, the intensity of CeO_2 diffraction peaks gradually attenuated with Pd content (see Fig. 1d), likely due to the contrast matching effect resulting from a site-specific deposition of Pd particles on CeO_2 surface [38] (see more discussion below).

The PZC values of the samples are listed in Table 1. The PZC of SBA-15 was measured to be 2.7, in accordance with previously reported values of SiO_2 [21,22]. Increasing Ce amount from 2.34 wt.% to 6.76 wt.% led to monotonously increased PZCs of the samples from 2.7 to 4.8, which gradually approached that of CeO_2 (6.6), reflecting the successful introduction of CeO_2 to SBA-15.

To understand the composition and chemical state of Pd in the catalysts, XPS analysis was conducted and the XPS spectra of the samples in the Pd 3d region are compared in Fig. 2. It was very clear that the peaks of the catalysts were highly asymmetric, implying the

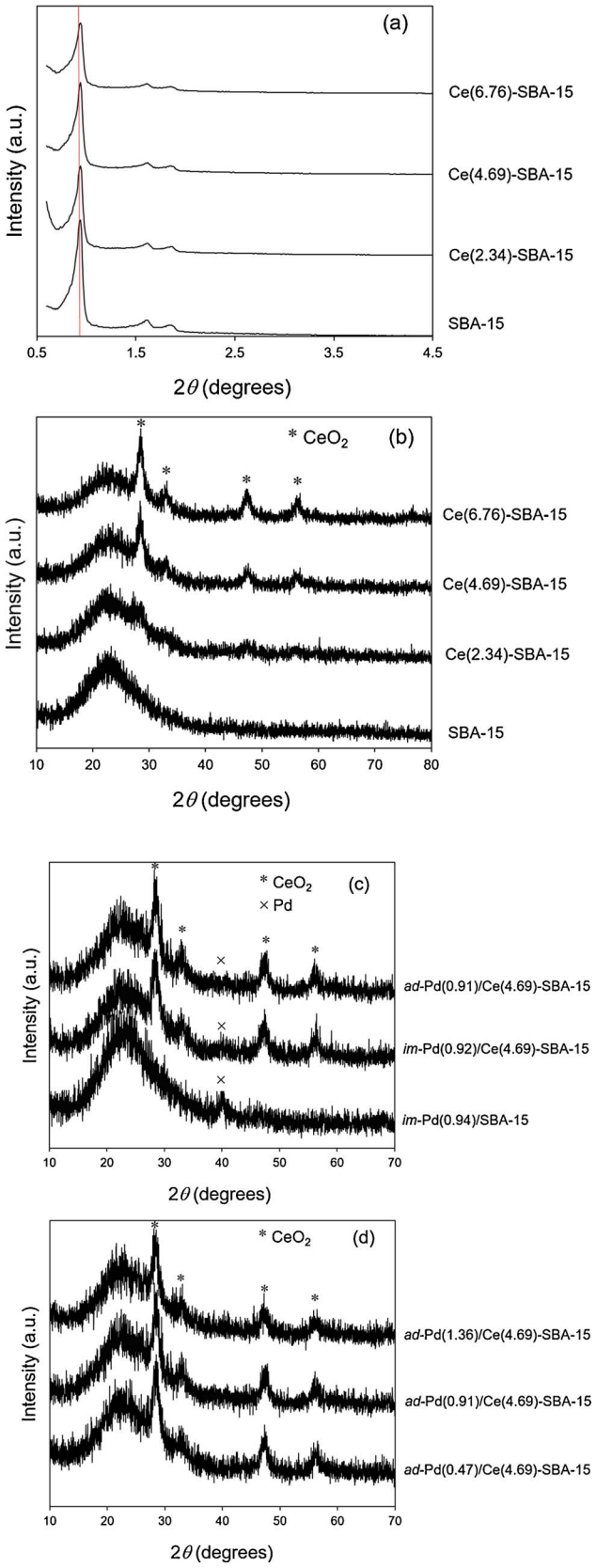

Fig. 1. (a) Small angle and (b), (c), (d) large range XRD patterns of the supports and catalysts.

Table 1
PZC values of the SBA-15, CeO_2 modified SBA-15 and CeO_2.

Samples	PZC
SBA-15	2.7
Ce(2.34)-SBA-15	3.8
Ce(4.69)-SBA-15	4.0
Ce(6.76)-SBA-15	4.8
CeO_2	6.6

coexistence of multiple Pd species in the samples. Thus, deconvolution was conducted on the XPS profiles and the obtained parameters are listed in Table 2. All the samples could be fitted into two doublets with binding energies in the Pd $3d_{5/2}$ region around 335.9 and 337.6 eV, attributed to metallic and positively charged Pd, respectively [39]. For *im*-Pd(0.94)/SBA-15, the content of Pd° was markedly higher than that of $Pd^{\delta+}$ with a ratio of $Pd^{\circ}/Pd^{\delta+}$ of 4.93. In contrast, much lower $Pd^{\circ}/Pd^{\delta+}$ ratios were identified in *im*-Pd(0.92)/Ce(4.69)-SBA-15 (0.76) and *ad*-Pd(0.91)/Ce(4.69)-SBA-15 (0.43), with the lowest one in *ad*-Pd (0.91)/Ce(4.69)-SBA-15. The very low $Pd^{\circ}/Pd^{\delta+}$ ratio was characteristic of enriched cationic Pd species on the catalyst surface as a consequence of strong metal-support interactions [40,41]. In general, very weak interactions between noble metals (*e.g.*, Au, Pd, and Pt) and SiO_2 were experimentally and theoretically observed [15,42,43], as also reflected by the very high $Pd^{\circ}/Pd^{\delta+}$ ratio in *im*-Pd(0.94)/SBA-15. On the contrary, CeO_2 is a reducible oxide and apt to invoke strong metal-support interactions, leading to electron transfer from noble metals to CeO_2 [13,44]. Notably, the binding energy characteristic of positive charged Pd was even higher than that of PdO, reflecting a very strong metal-support interaction. Such high binding energy values of Pd were previously observed (see more data in Table S2, SI). Accordingly, the low $Pd^{\circ}/Pd^{\delta+}$ ratio in *ad*-Pd(0.91)/Ce(4.69)-SBA-15 again confirmed the site-specific deposition of Pd particles on CeO_2 moieties. The strong metal-support interactions between Pd and CeO_2 moieties could be further evidenced by the decreased $Pd^{\circ}/Pd^{\delta+}$ ratio from 1.02 to 0.29 with the increase of CeO_2 modification amount from 2.34 wt.% to 6.76 wt.% (see Fig. 2b). Additionally, decreasing Pd loading content would lead to decreased Pd particle size and thus enhanced metal-support interaction, resulting in more marked cationization of Pd, as reflected by the decrease in $Pd^{\circ}/Pd^{\delta+}$ ratio from 2.75 to 0.22 with the decrease of Pd content from 1.36 wt.% to 0.47 wt.% (see Fig. 2c).

The TEM images of the samples are shown in Fig. S5, SI. Ce-SBA-15 and supported Pd catalysts displayed ordered mesoporous structures, indicative of well-remained structures of SBA-15 after CeO_2 modification and Pd loading, which was in line with BET and XRD results. At Ce amount of 2.34 wt.%, distinct CeO_2 particles were observed with random distribution in the channels and on the external surface of SBA-15. Increasing CeO_2 modification amount led to gradual growth of CeO_2 particles with irregular shapes. For supported Pd catalysts, clear Pd particles were only observed on *im*-Pd(0.94)/SBA-15, with particle size ranging from 3.1 to 8.9 nm, reflecting that most Pd particles were located on the external surface of SBA-15 due to much larger Pd particle size than the pore size of SBA-15. However, for Pd catalysts supported on Ce-SBA-15 Pd particles were not clearly visible because it was very difficult to differentiate Pd particles from CeO_2 moieties, or Pd particles were too small to identify.

To further observe Pd distributions in the catalysts, EDS elemental mapping was conducted on *ad*-Pd(0.91)/Ce(4.69)-SBA-15 and *im*-Pd (0.92)/Ce(4.69)-SBA-15, and the images are shown in Fig. 3. For *ad*-Pd (0.91)/Ce(4.69)-SBA-15, a similar distribution of Pd element to that of Ce element was observed, and the signal of elemental Pd diminished in the region without Ce signal. The excellent overlapping of elemental Pd with Ce was indicative of a close contact of Pd with CeO_2, verifying the site-specific deposition of Pd on CeO_2 moieties rather than on SBA-15 [45]. As for *im*-Pd(0.92)/Ce(4.69)-SBA-15, uniform distribution of elemental Pd was observed which was independent on that of elemental Ce, reflecting a random distribution of Pd on both CeO_2 and SBA-15 surface.

The dispersions and particle sizes of Pd in the catalysts were further determined by H_2 chemisorption and the results are listed in Table 2. For *im*-Pd(0.94)/SBA-15, Pd dispersion was calculated to be 16.3%, while Pd dispersions in *im*-Pd(0.92)/Ce(4.69)-SBA-15 and *ad*-Pd(0.91)/Ce(4.69)-SBA-15 were 39.6% and 53.3%, much higher than that in *im*-Pd(0.94)/SBA-15. In comparison with *im*-Pd(0.92)/Ce(4.69)-SBA-15, considerably higher Pd dispersion was obtained on *ad*-Pd(0.91)/Ce (4.69)-SBA-15, resulting from a stronger interaction between Pd and CeO_2 moieties in the catalyst prepared using the SEA method. Additionally, for the *ad*-Pd/Ce-SBA-15 catalysts, increasing CeO_2 modification amount enhanced Pd dispersion, again confirming the positive relationship between Pd dispersion and the metal-support interaction. For the *ad*-Pd/Ce(4.69)-SBA-15 catalyst, increasing Pd content from 0.47 wt.% to 1.36 wt.% resulted in a decreased Pd dispersion from 95.0% to 38.5%, due to gradually growing Pd particles and thus attenuated metal-support interaction. In parallel, the average particle sizes of Pd in the catalysts could be calculated using H_2 chemisorption data. The average Pd particle size in *im*-Pd(0.94)/SBA-15 was 6.0 nm, close to that measured by TEM. The average Pd particle sizes were 1.8 and 2.5 nm in *ad*-Pd(0.91)/Ce(4.69)-SBA-15 and *im*-Pd(0.92)/Ce(4.69)-SBA-15, respectively. Furthermore, in the *ad*-Pd/Ce-SBA-15 catalysts increasing CeO_2 amount led to decreased Pd particle size from 4.0 to 1.4 nm, and decreasing Pd content resulted in decreased Pd particle size from 2.7 to 1.0 nm. Notably, the contribution of the confinement effect from SBA-15 pores for the presence of very small Pd particles in *ad*-Pd/Ce-SBA-15 samples could be excluded, as reflected by the presence of very large Pd particles in *im*-Pd(0.94)/SBA-15.

Based on above characterization results, it could be concluded that the structural properties of supported Pd catalysts were strongly dependent on catalyst support and preparation method. In comparison with *im*-Pd(0.92)/Ce(4.69)-SBA-15 and *ad*-Pd(0.91)/Ce(4.69)-SBA-15, very low Pd dispersion was obtained on *im*-Pd(0.94)/SBA-15 due to the weak metal-support interaction. For supported Pd catalyst prepared by the impregnation method (*i.e.*, *im*-Pd(0.92)/Ce(4.69)-SBA-15), during the impregnation process Pd precursor ion $[PdCl_4]^{2-}$ was randomly located on CeO_2 moieties and SBA-15 surface, leading to the formation of large Pd particles on SiO_2 surface in addition to small Pd particles on CeO_2 moieties as a result of weak interactions between Pd and SiO_2. As for the preparation of *ad*-Pd(0.91)/Ce(4.69)-SBA-15, the solution pH was adjusted to 3.6, between the PZC value of SBA-15 and CeO_2, giving rise to positively charged CeO_2 moieties and negatively charged SBA-15 surface. Hence, $[PdCl_4]^{2-}$ ions were site-specifically adsorbed on CeO_2 moieties rather than SBA-15 surface, resulting in high Pd dispersion and small sized Pd particles owing to the presence of strong metal-support interactions. The different preparation methods for supported Pd catalysts are described in Scheme 1.

3.2. Liquid phase catalytic reduction of bromate

3.2.1. Effect of preparation method and support

The catalytic reduction of bromate over the catalysts are compared in Fig. 4. For all bromate reduction reactions, the sum of bromate and bromide concentrations were found to be equal to the initial bromate concentrations (results presented in Fig. S6, SI), reflecting bromide as the single reduction product. As for catalytic activities of the catalysts, nearly negligible bromate conversion (about 5% after reaction for 2 h) was observed on *im*-Pd(0.94)/SBA-15. In contrast, bromate was removed by 71% within 2 h on *im*-Pd(0.92)/Ce(4.69)-SBA-15 and was completely reduced within 50 min on *ad*-Pd(0.91)/Ce(4.69)-SBA-15, giving a decreasing catalytic activity order: *ad*-Pd(0.91)/Ce(4.69)-SBA-15 > *im*-Pd(0.92)/Ce(4.69)-SBA-15 > *im*-Pd(0.94)/SBA-15. The very different catalytic performances of Pd catalysts supported on SBA-15 and CeO_2 modified SBA-15 indicated the crucial role of CeO_2

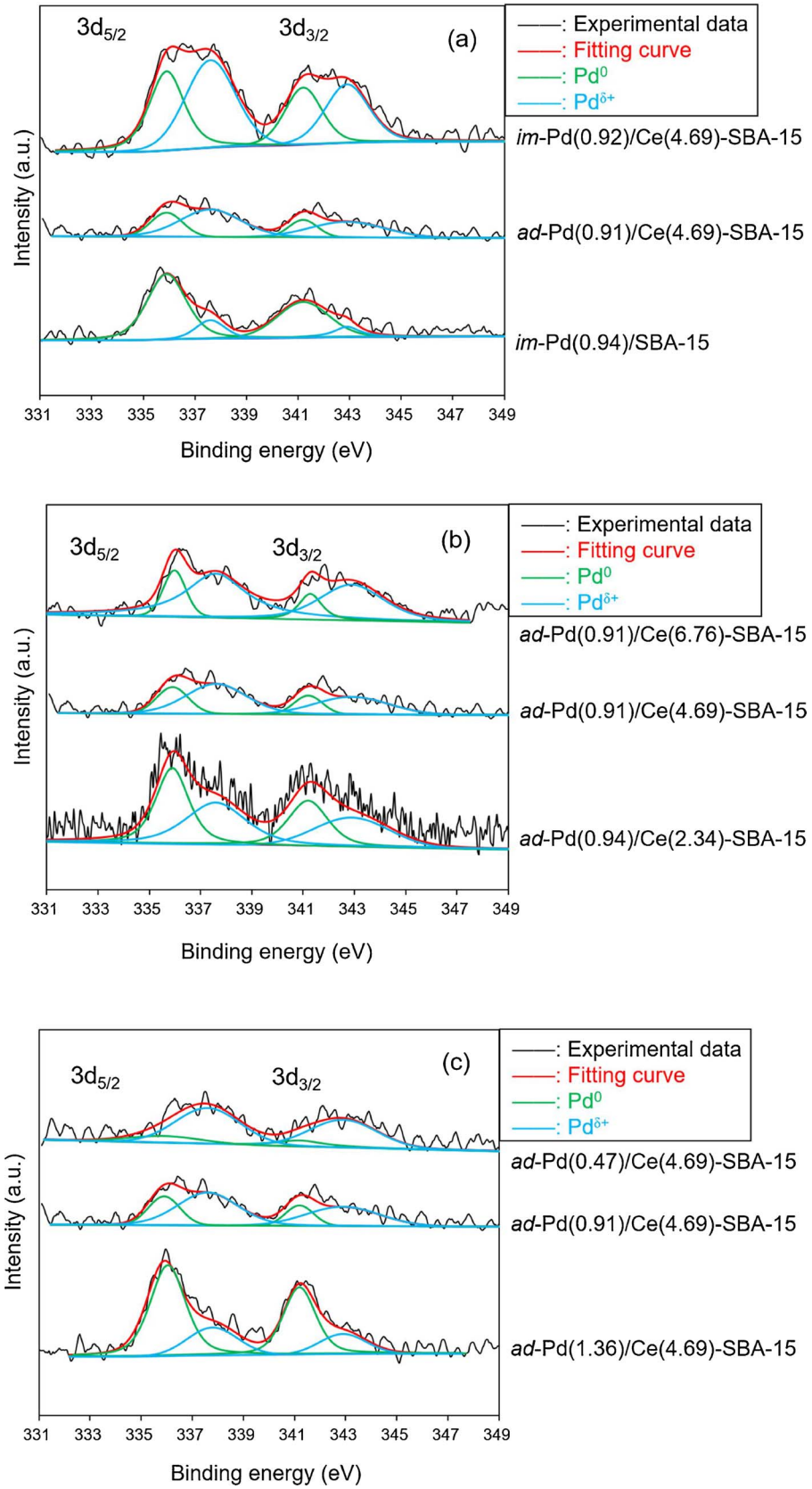

Fig. 2. XPS spectra of (a) Pd catalysts prepared by different methods and supported on different supports, and *ad*-Pd/Ce-SBA-15 catalysts with (b) varied Ce modification amounts, (c) varied Pd loading amounts in the Pd 3d region.

Table 2
Properties and catalytic performances of the catalysts.

Catalysts	Pd [a] (wt. %)	Ce [a] (wt. %)	Pd/Pd$^{\delta+}$ ratio [b]	d_1 [c] (nm)	d_2 [d] (nm)	D[e] (%)	Initial activity [f] (mM g_{cat}^{-1} h^{-1})	TOF HYPERLINK \l "tFoot27" \h [g] (s^{-1})
im-Pd(0.94)/SBA-15	0.94	–	4.93	5.9	6.0	16.3	3.7	0.03
im-Pd(0.92)/Ce(4.69)-SBA-15	0.92	4.69	0.76	–	2.5	39.6	54.5	0.15
ad-Pd(0.91)/Ce(4.69)-SBA-15	0.91	4.69	0.43	–	1.8	53.3	210.7	0.45
ad-Pd(0.47)/Ce(4.69)-SBA-15	0.47	4.69	0.22	–	1.0	95.0	107.6	0.25
ad-Pd(1.36)/Ce(4.69)-SBA-15	1.36	4.69	2.75	–	2.7	38.5	237.9	0.47
ad-Pd(0.94)/Ce(2.34)-SBA-15	0.94	2.34	1.02	–	4.0	26.0	59.0	0.26
ad-Pd(0.91)/Ce(6.76)-SBA-15	0.91	6.76	0.29	–	1.4	68.5	211.9	0.40

[a] Determined by ICP-AES.
[b] Calculated by XPS.
[c] Calculated by TEM.
[d] Calculated by H_2 chemisorption.
[e] Pd dispersion, determined by H_2 chemisorption.
[f] Reaction conditions: pH 5.6, catalyst dosage: 0.028 g l^{-1}, initial bromate concentration: 0.60 mM.
[g] Initial TOFs of exposed Pd sites on the catalysts. Reaction conditions: pH 5.6, catalyst dosage: 0.028 g l^{-1}, initial bromate concentration: 0.60 mM.

modification for catalytic bromate reduction. Accordingly, our previous study showed that highly effective bromate reduction was also observed on Pd/CeO_2 [13]. Notably, *ad*-Pd(0.91)/Ce(4.69)-SBA-15 exhibited a comparable catalytic activity to Pd/CeO_2 for bromate reduction. Considering that *ad*-Pd(0.91)/Ce(4.69)-SBA-15 had a Ce loading of 4.69 wt. %, highly effective utilization of CeO_2 could be achieved in the catalyst. For heterogeneous catalytic reactions, the adsorption of reactant on catalyst surface is recognized as a prerequisite step. Because the reaction occurred at pH of 5.6, the surface of SBA-15 with a PZC of 2.7 was negatively charged, and electrostatic repulsive interaction was expected between anionic bromate and catalyst surface, suppressing the access of bromate to Pd surface. Hence, negligible activity was observed on *im*-Pd (0.94)/SBA-15. In contrast to SBA-15, CeO_2 had a much higher PZC (6.6), and CeO_2 modification led to increased PZC of modified SBA-15 (see Table 1). At reaction pH (5.6), CeO_2 moieties in Ce-SBA-15 were positively charged, which enhanced the adsorption of anionic bromate on catalyst surface, leading to increased catalytic activities of *im*-Pd (0.92)/Ce(4.69)-SBA-15 and *ad*-Pd(0.91)/Ce(4.69)-SBA-15. Notably, the initial activity of *ad*-Pd(0.91)/Ce(4.69)-SBA-15 was 210.7 mM g_{cat}^{-1} h^{-1}, much higher than that of *im*-Pd(0.92)/Ce(4.69)-SBA-15 (54.5 mM g_{cat}^{-1} h^{-1}) (see Table 2). Characterization results showed that *ad*-Pd(0.91)/Ce(4.69)-SBA-15 had a higher Pd dispersion and smaller average Pd particle size, giving rise to a higher catalytic activity than that of *im*-Pd(0.92)/Ce(4.69)-SBA-15. For clearer understanding,

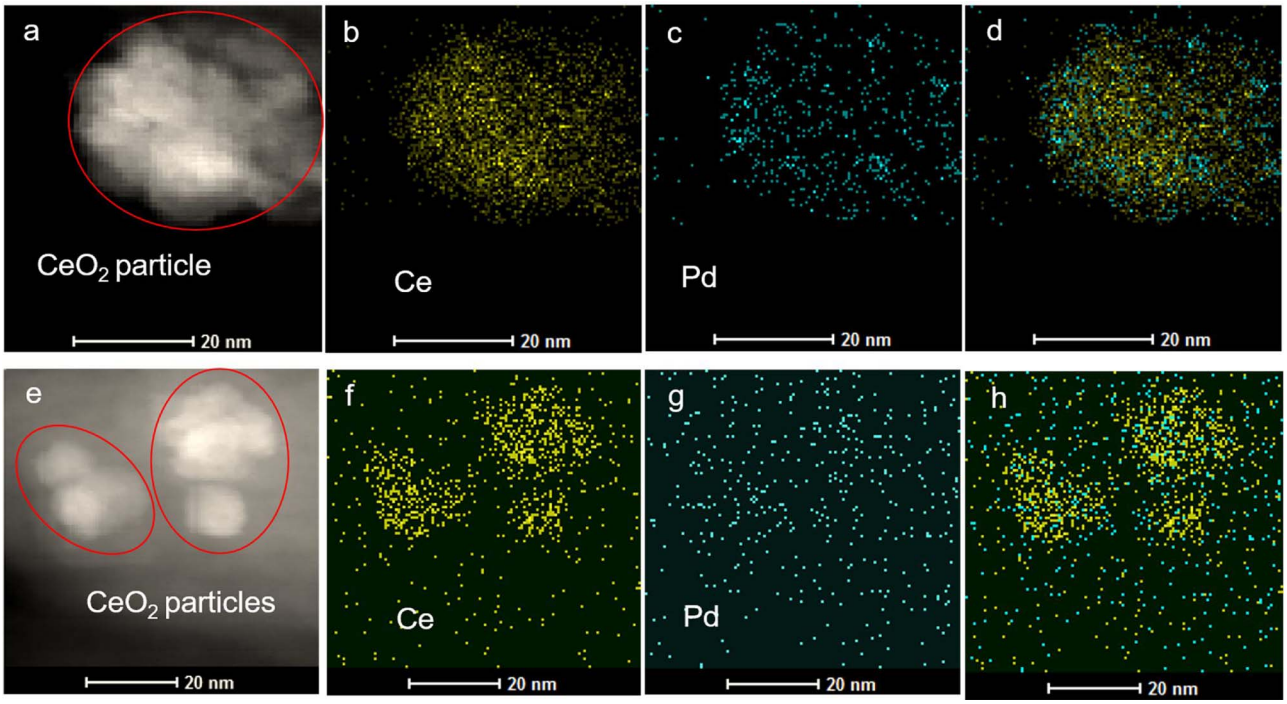

Fig. 3. (a) HAADF-TEM image of a CeO_2 particle on *ad*-Pd(0.91)/Ce(4.69)-SBA-15 and the corresponding EDS elemental mapping of (b) Ce element (yellow), (c) Pd element (blue), (d) the overlapping of Ce and Pd elements, (e) HAADF-TEM image of CeO_2 particles on *im*-Pd(0.92)/Ce(4.69)-SBA-15 and the corresponding EDS elemental mapping of (f) Ce element (yellow), (g) Pd element (blue), and (h) the overlapping of Ce and Pd element.

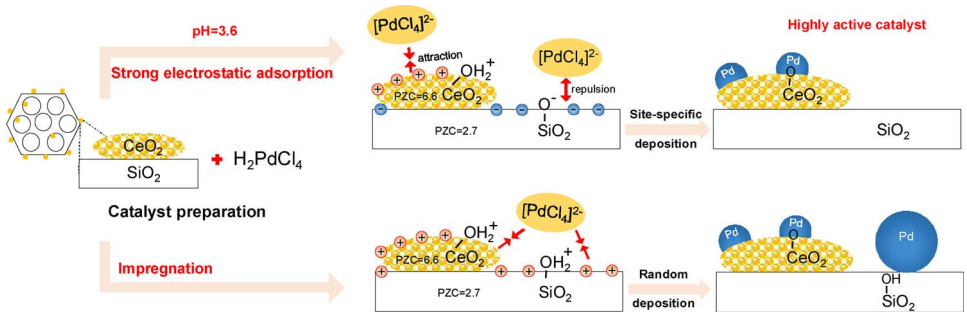

Scheme 1. Preparation of supported Pd catalysts on Ce-SBA-15 using the strong electrostatic adsorption and impregnation methods.

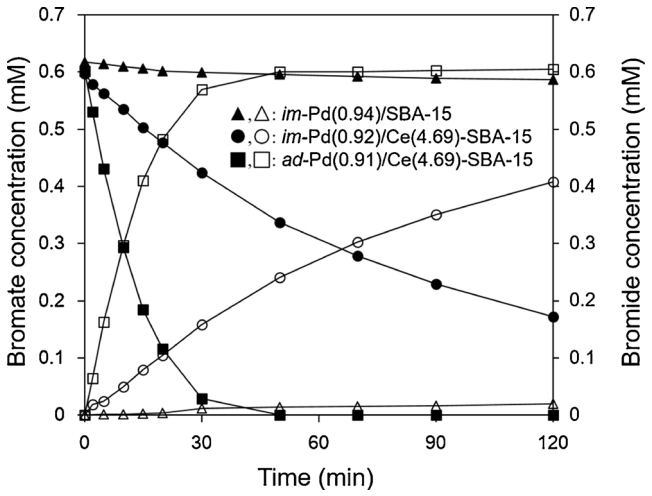

Fig. 4. Liquid phase catalytic reduction of bromate on Pd catalysts prepared by different methods and supported on different supports. Filled symbols represent bromate concentrations and open symbols represent bromide concentrations. Reaction conditions: reaction pH 5.6, catalyst dosage: 0.028 g l^{-1}, initial bromate concentration: 0.60 mM.

the turnover frequency (TOF) values of exposed Pd sites in *im*-Pd(0.92)/Ce(4.69)-SBA-15 and *ad*-Pd(0.91)/Ce(4.69)-SBA-15 were compared. The TOF values were obtained by calculating the initial bromate conversion normalized by exposed Pd sites of the catalysts, and the numbers of exposed Pd sites in the catalysts were obtained using H_2 chemisorption data. The TOF values of *im*-Pd(0.92)/Ce(4.69)-SBA-15 and *ad*-Pd(0.91)/Ce(4.69)-SBA-15 were calculated to be 0.15 s^{-1} and 0.45 s^{-1}, reflecting a much higher activity of Pd site in *ad*-Pd(0.91)/Ce(4.69)-SBA-15 than that in *im*-Pd(0.92)/Ce(4.69)-SBA-15. Because under the reaction conditions SBA-15 and CeO_2 were negatively and positively charged respectively, only Pd particles located on CeO_2 moieties were accessible for anionic bromate due to electrostatic attractive interaction, whereas adsorption of bromate on Pd particles located on SBA-15 was inhibited because of repulsive interaction, as verified by the negligible bromate conversion on *im*-Pd(0.94)/SBA-15. For *im*-Pd(0.92)/Ce(4.69)-SBA-15, Pd particles randomly dispersed on the surface of both CeO_2 moieties and SiO_2. Hence, only partial of Pd sites participated in the reaction. In contrast, for *ad*-Pd(0.91)/Ce(4.69)-SBA-15, Pd particles were located on CeO_2 moieties, and nearly all Pd sites were accessible for anionic bromate, accounting for the higher TOF of Pd sites in *ad*-Pd(0.91)/Ce(4.69)-SBA-15.

The importance of bromate adsorption could be further verified by investigating the influence of initial bromate concentration on bromate reduction on *ad*-Pd(0.91)/Ce(4.69)-SBA-15, and the results are presented in Fig. 5. Increasing initial bromate concentration led to increased initial reduction rate, suggesting a positive correlation between the reaction rate and the adsorbed bromate concentration. The results were further fitted to the Langmuir-Hinshelwood model [46,47]:

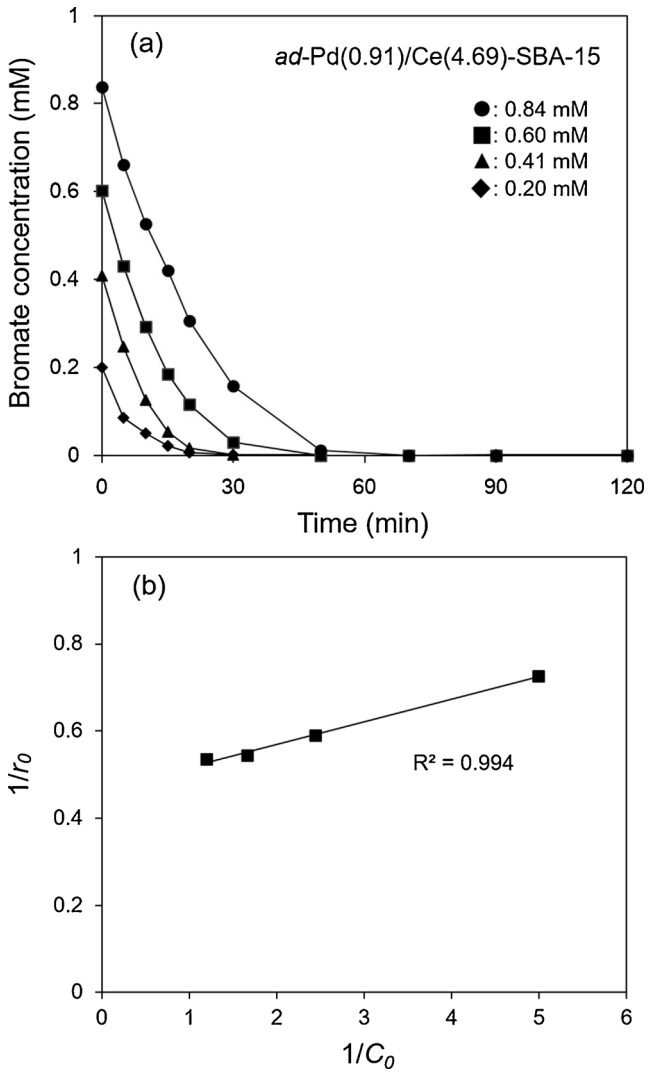

Fig. 5. (a) Liquid phase catalytic reduction of bromate on *ad*-Pd(0.91)/Ce(4.69)-SBA-15 with varied initial bromate concentrations, and (b) linear plot of $1/r_0$ versus $1/C_0$ for the catalytic reduction of bromate, and the Line fitting used the Langmuir-Hinshelwood model. Reaction conditions: reaction pH 5.6, catalyst dosage: 0.028 g l^{-1}.

$$r_0 = k\theta_s = k\frac{bC_0}{1 + bC_0} \quad (1)$$

$$\frac{1}{r_0} = \frac{1}{kbC_0} + \frac{1}{k} \quad (2)$$

Where r_0 is the initial bromate reduction rate, θ_s is the surface bromate coverage on catalyst, C_0 is the initial bromate concentration, b is bromate adsorption constant, and k is the reduction rate constant.

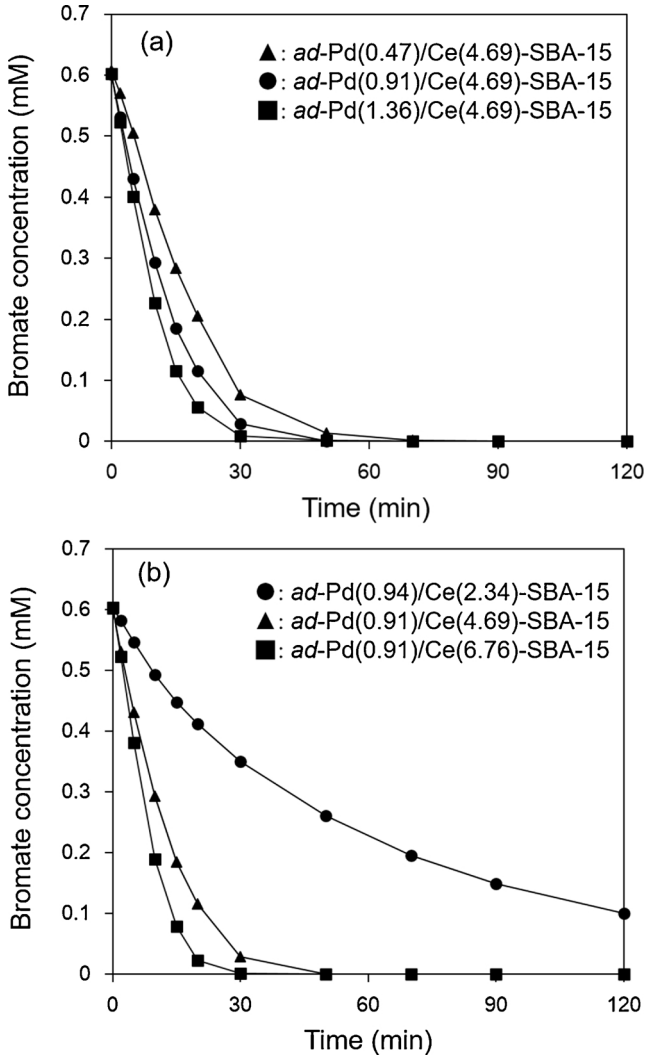

Fig. 6. Liquid phase catalytic reduction of bromate on*ad*-Pd/Ce-SBA-15 catalysts with (a) varied Pd loading amounts, and (b) varied Ce modification amounts. Reaction conditions: reaction pH 5.6, catalyst dosage: 0.028 g l^{-1}, initial bromate concentration: 0.60 mM.

The relationship between C_o and r_o plotted as $1/C_o$ versus $1/r_o$ is presented in Fig. 5b. The plot of $1/C_o$ versus $1/r_o$ displayed a good linear relationship, indicating that catalytic bromate reduction well followed the Langmuir-Hinshelwood model. The results also revealed that the conversion of adsorbed bromate on catalyst surface was the rate controlling step in the liquid phase catalytic reduction of bromate, confirming the importance of bromate adsorption on catalyst surface.

3.2.2. Effect of the Pd content on the catalytic reduction of bromate

The Pd content in the catalyst may impact its catalytic activity. The Pd catalysts supported on Ce(4.69)-SBA-15 with three Pd contents (0.47 wt.%, 0.91 wt.% and 1.36 wt.%) prepared using the SEA method were applied in bromate reduction, and results are compiled in Fig. 6a. Increasing Pd content from 0.47 to 1.36 wt.% led to increased initial bromate reduction rate from 107.6 to 237.9 mM g_{cat}^{-1} h^{-1}. The enhanced catalytic activity of *ad*-Pd/Ce(4.69)-SBA-15 was primarily ascribed to increased catalytic active sites with Pd content. A deep insight could be gained from TOF values of exposed Pd sites of the catalysts. The TOF values of *ad*-Pd(0.47)/Ce(4.69)-SBA-15, *ad*-Pd(0.91)/Ce(4.69)-SBA-15 and *ad*-Pd(1.36)/Ce(4.69)-SBA-15 were calculated to be 0.25, 0.45, and 0.47 s^{-1}, respectively (see Table 2). This trend was likely associated with the structural properties of Pd particles in the catalysts. In principle, large-sized Pd particles favored effective H_2 activation in catalytic hydrogenation reactions due to enhanced solubility of H_2 and formation of β-PdH species [12,20,48,49]. As reflected by H_2 chemisorption, increasing Pd content led to formation of large Pd particles in the *ad*-Pd/Ce(4.69)-SBA-15 catalysts, thus resulting in enhanced TOF for bromate reduction. Accordingly, higher TOF values were previously observed on larger Pd particles for some catalytic hydrogenation reactions [12,20,49,50].

3.2.3. Effect of the CeO_2 modification amount on the catalytic reduction of bromate

As discussed above, CeO_2 modification markedly enhanced the activity of the catalyst. Accordingly, modification amount of CeO_2 in the *ad*-Pd/Ce-SBA-15 catalyst likely affected catalytic bromate reduction. Hence, the catalytic bromate reduction was carried out on *ad*-Pd/Ce-SBA-15 with CeO_2 modification amount varying from 2.34 wt.% to 6.76 wt.%, and the results are compared in Fig. 6b. The initial activities for bromate reduction were 59.0, 210.7 and 211.9 mM g_{cat}^{-1} h^{-1}, for *ad*-Pd(0.94)/Ce(2.34)-SBA-15, *ad*-Pd(0.91)/Ce(4.69)-SBA-15 and *ad*-Pd(0.91)/Ce(6.76)-SBA-15, respectively. The significantly improved catalytic activity with Ce amount again verified a strong influence of CeO_2 modification on the catalytic performance. The TOF values of *ad*-Pd(0.94)/Ce(2.34)-SBA-15, *ad*-Pd(0.91)/Ce(4.69)-SBA-15 and *ad*-Pd(0.91)/Ce(6.76)-SBA-15 were 0.26, 0.45 and 0.40 s^{-1}, respectively. Among the three catalysts, *ad*-Pd(0.94)/Ce(2.34)-SBA-15 had a largest Pd particle size, but a lowest TOF value, which seemed contradictory to above observed trend. This discrepancy could be interpreted in terms of impact of CeO_2 modification on bromate adsorption. As already demonstrated, CeO_2 modification effectively enhanced bromate adsorption, and thus catalytic activity. At a low CeO_2 modification amount, increasing CeO_2 amount remarkably facilitated bromate adsorption, likely playing a more important role than H_2 activation on Pd particles. At a high CeO_2 modification amount, the enhancement of bromate adsorption with CeO_2 amount gradually alleviated, and H_2 activation on Pd sites dominated, as confirmed by the higher TOF of Pd site in *ad*-Pd(0.91)/Ce(4.69)-SBA-15 than in *ad*-Pd(0.91)/Ce(6.76)-SBA-15.

4. Conclusions

In this work, a series of supported Pd catalysts on CeO_2 modified SBA-15 with different Pd loading and CeO_2 modification amounts were prepared using the SEA method. For comparison purpose, Pd catalysts supported on SBA-15 and CeO_2 modified SBA-15 were prepared using the impregnation method. Liquid phase catalytic hydrogenation of bromate on the catalysts was investigated. Due to the higher PZC of CeO_2 than that of SBA-15, CeO_2 modification results in increased PZC of Ce-SBA-15. For the preparation of Pd catalyst with Ce-SBA-15 as the support using the SEA method, Pd precursor (*i.e.*, $[PdCl_4]^{2-}$ anion) is preferentially adsorbed on positively charged CeO_2 moieties instead of negatively charged SiO_2. Hence, site-specific Pd deposition on CeO_2 moieties is achieved in the *ad*-Pd/Ce-SBA-15 catalysts, as reflected by the perfect overlapping of elemental Pd mapping with elemental Ce mapping in a*d*-Pd(0.91)/Ce(4.69)-SBA-15. In contrast, random distribution of Pd on both CeO_2 moieties and SiO_2 is obtained in *im*-Pd(0.92)/Ce(4.69)-SBA-15. Accordingly, much higher Pd dispersion and stronger cationization of Pd are identified on a*d*-Pd(0.91)/Ce(4.69)-SBA-15 than on *im*-Pd(0.92)/Ce(4.69)-SBA-15 and *im*-Pd(0.94)/SBA-15. The liquid phase catalytic hydrogenation of bromate follows the Langmuir-Hinshelwood model, indicating that the reduction of adsorbed bromate is the rate-controlling step. Accordingly, negligible bromate conversion is observed on *im*-Pd(0.94)/SBA-15 because of electrostatic repulsive interaction between SBA-15 and anionic bromate. In contrast, effective bromate reduction is achieved on *im*-Pd(0.92)/Ce(4.69)-SBA-15 and a*d*-Pd(0.91)/Ce(4.69)-SBA-15, while a higher catalytic activity is obtained on a*d*-Pd(0.91)/Ce(4.69)-SBA-15 than on *im*-Pd(0.92)/Ce(4.69)-SBA-15. This is because in a*d*-Pd(0.91)/Ce(4.69)-SBA-15 Pd sites are exclusively located on CeO_2 moieties, fully

accessible for bromate due to electrostatic attractive interaction between bromate and CeO_2 moieties. Additionally, increasing CeO_2 modification amount leads to improved catalytic activity as a result of enhanced bromate adsorption and Pd dispersion.

Acknowledgements

The financial support from the National Natural Science Foundation of China (no. 21577056 and 21507056), and the Natural Science Foundation of Jiangsu Province (BK20150568) is gratefully acknowledged.

Appendix A. Supplementary data

Supplementary material related to this article can be found, in the online version, at doi:https://doi.org/10.1016/j.apcatb.2018.02.009.

References

[1] G.A. Boorman, V. Dellarco, J.K. Dunnick, R.E. Chapin, S. Hunter, F. Hauchman, H. Gardner, M. Cox, R.C. Sills, Environ. Health Persp. 107 (1999) 207–217.
[2] World Health Organization, WHO Guide Lines for Drinking Water Quality, Geneva, Switzerland (1996).
[3] United States Environmental Protection Agency, National Primary Drinking Water Regulations: Stage 2 Disinfectants and Disinfection Byproducts Rule, Federal Register, (2003).
[4] A.N. Davidson, J. Chee-Sanford, H.Y. Lai, C.-H. Ho, J.B. Klenzendorf, M.J. Kirisits, Water Res. 45 (2011) 6051–6062.
[5] J. Xiao, W. Yang, Q. Li, Appl. Catal. B Environ. 218 (2017) 111–118.
[6] Q. Wang, S. Snyder, J. Kim, H. Choi, Environ. Sci. Technol. 43 (2009) 3292–3299.
[7] R. Mao, X. Zhao, H. Lan, H. Liu, J. Qu, Appl. Catal. B Environ. 160–161 (2014) 179–187.
[8] N. Barrabés, J.S.á Appl, Catal. B Environ. 104 (2011) 1–5.
[9] H. Chen, Y. Shao, Z. Xu, H. Wan, Y. Wan, S. Zheng, D. Zhu, Appl. Catal. B Environ. 105 (2011) 255–262.
[10] D.B. Thakur, R.M. Tiggelaar, Y. Weber, J.G.E. Gardeniers, K. Seshan, Appl. Catal. B Environ. 102 (2011) 243–250.
[11] J. Zhou, Y. Han, W. Wang, Z. Xu, H. Wan, D. Yin, S. Zheng, D. Zhu, Appl. Catal. B Environ. 134–135 (2013) 222–230.
[12] J. Zhou, K. Wu, W. Wang, Z. Xu, H. Wan, S. Zheng, Appl. Catal. A Gen. 470 (2014) 336–343.
[13] J. Zhou, K. Wu, W. Wang, Y. Han, Z. Xu, H. Wan, S. Zheng, D. Zhu, Appl. Catal. B Environ. 162 (2015) 85–92.
[14] A.E. Palomares, C. Franch, T. Yuranova, L. Kiwi-Minsker, E. García-Bordeje, S. Derrouiche, Appl. Catal. B Environ. 146 (2014) 186–191.
[15] Q. Fu, T. Wagner, Surf. Sci. Rep. 62 (2007) 431–498.
[16] J.H. Kwak, J. Hu, D. Mei, C.-W. Yi, D.H. Kim, C.H.F. Peden, L.F. Allard, J. Szanyi, Science 325 (2009) 1670–1673.
[17] S. Bernal, J. Calvino, M. Cauqui, J. Gatica, C. Larese, J. Pérez Omil, J. Pintado, Catal. Today 50 (1999) 175–206.
[18] D. Zhao, J. Feng, Q. Huo, N. Melosh, G. Fredrickson, B. Chmelka, G. Stucky, Science 279 (1998) 548–552.
[19] B. Huang, X. Li, S. Ji, B. Lang, F. Habimana, C. Li, J. Nat. Gas 17 (2008) 225–231.
[20] H. Chen, Z. Xu, H. Wan, J. Zheng, D. Yin, S. Zheng, Appl. Catal. B Environ. 96 (2010) 307–313.
[21] R. Huang, H. Yan, L. Li, D. Deng, Y. Shu, Q. Zhang, Appl. Catal. B Environ. 106 (2011) 264–271.
[22] L. Jiao, J.R. Regalbuto, J. Catal. 260 (2008) 342–350.
[23] Y.D. Bi, W. Zhang, H.Y. Xu, W.Z. Li, Catal. Lett. 119 (2007) 126–133.
[24] C.K. Krishnan, K. Nakamura, H. Hirata, M. Ogura, Phys. Chem. Chem. Phys. 12 (2010) 7513–7520.
[25] J. Tao, L. Zhao, C. Dong, Q. Lu, X. Du, E. Dahlquist, Energies 6 (2013) 3284–3296.
[26] A. Trovarelli, C. de Leitenburg, M. Boaro, G. Dolcetti, Catal. Today 50 (1999) 353–367.
[27] K. Binnemans, P.T. Jones, B. Blanpain, T. Van Gerven, Y. Yang, A. Walton, M. Buchert, J. Clean. Prod. 51 (2013) 1–22.
[28] K. Binnemans, P.T. Jones, K. Van Acker, B. Blanpain, B. Mishra, D. Apelian, JOM 65 (2013) 846–848.
[29] W.A. Spieker, J.R. Regalbuto, Chem. Eng. Sci. 56 (2001) 3491–3504.
[30] J.T. Miller, M. Schreier, A.J. Kropf, J.R. Regalbuto, J. Catal. 225 (2004) 203–212.
[31] L. Jiao, J.R. Regalbuto, J. Catal. 260 (2008) 329–341.
[32] M.A. Aramendia, V. Borau, C. Jimenez, J.M. Marinas, A. Moreno, Colloids Surf. A 106 (1996) 161–165.
[33] J. Wang, L. Gao, Nanostruct. Mater. 11 (1999) 451–457.
[34] Z. Luan, E.M. Maes, P.A.W. Van Der Heide, D. Zhao, R.S. Czernuszewicz, L. Kevan, Chem. Mater. 11 (1999) 3680–3686.
[35] X.K. Li, W.J. Ji, J. Zhao, Z.B. Zhang, C.T. Au, J. Catal. 238 (2006) 232–241.
[36] C.A. Fyfe, G. Fu, J. Am. Chem. Soc. 117 (1995) 9709–9714.
[37] K.R. Priolkar, P. Bera, P.R. Sarode, M.S. Hegde, S. Emura, R. Kumashiro, N.P. Lalla, Chem. Mater. 14 (2002) 2120–2128.
[38] L. Mercier, T.J. Pinnavaia, Chem. Mater. 12 (2000) 188–196.
[39] G.J. Zhang, Y.N. Wang, X. Wang, Y. Chen, Y.M. Zhou, Y.W. Tang, L.D. Lu, J.C. Bao, T.H. Lu, Appl. Catal. B Environ. 102 (2011) 614–619.
[40] S. Hinokuma, H. Fujii, M. Okamoto, K. Ikeue, M. Machida, Chem. Mater. 22 (2010) 6183–6190.
[41] X. Qian, Y. Kuwahara, K. Mori, H. Yamashita, Chem. –Eur. J. (2014) 15746–15752.
[42] N. Lopez, F. Illas, G. Pacchioni, J. Am. Chem. Soc. 121 (1999) 813–821.
[43] J.M. Antonietti, M. Michalski, U. Heiz, H. Jones, K.H. Lim, N. Rosch, A. Del Vitto, G. Pacchioni, Phys. Rev. Lett. 94 (2005) 213–402.
[44] A. Trovarelli, Catal. Rev. 38 (1996) 439–520.
[45] Y. Guo, J. Zou, X. Shi, P. Rukundo, Z. Wang, A.C.S. Sustain, Chem. Eng. 5 (2017) 2330–2338.
[46] A. Pintar, J. Batista, J. Levec, T. Kajiuchi, Appl. Catal. B Environ. 11 (1996) 81–98.
[47] Z.M. de Pedro, J.A. Casas, L.M. Gomez-Sainero, J.J. Rodriguez, Appl. Catal. B Environ. 98 (2010) 79–85.
[48] C.E. Gigola, H.R. Aduriz, P. Bodnariuk, Appl. Catal. 27 (1986) 138.
[49] M.A. Aramendia, V. Borau, I.M. Garcia, C. Jimenez, J.M. Marinas, F.J. Urbano, Appl. Catal. B Environ. 20 (1999) 101–110.
[50] J.A. Baeza, L. Calvo, M.A. Gilarranz, A.F. Mohedano, J.A. Casas, J.J. Rodriguez, J. Catal. 293 (2012) 85–93.